Green Mass Production of Pure Nanodrugs via an Ice-Template-Assisted Strategy

Green Mass Production of Pure Nanodrugs via an Ice-Template-Assisted Strategy

Jinfeng Zhang[†,‡], Weidong Nie[†], Rui Chen[§], Jipsa Chelora[‡], Yingpeng Wan[‡], Xiao Cui[‡], Xiaohong Zhang[∥,], Wenjun Zhang[§], Xianfeng Chen[⊥], Hai-Yan Xie[†], and Chun-Sing Lee[‡,*]*

[†]School of Life Science, Beijing Institute of Technology, Beijing 100081, P. R. China.

[‡]Center of Super-Diamond and Advanced Films (COSDAF) & Department of Chemistry, City University of Hong Kong, 83 Tat Chee Avenue, Kowloon, Hong Kong SAR, P. R. China.

[§]Center of Super-Diamond and Advanced Films (COSDAF) & Department of Materials Science and Engineering, City University of Hong Kong, 83 Tat Chee Avenue, Kowloon, Hong Kong SAR, P. R. China.

[∥]Institute of Functional Nano & Soft Materials (FUNSOM), Jiangsu Key Laboratory for Carbon-Based Functional Materials & Devices, Soochow University, Suzhou, Jiangsu 215123, P. R. China.

[⊥]School of Engineering, Institute for Bioengineering, The University of Edinburgh, King's Buildings, Mayfield Road, Edinburgh EH9 3JL, United Kingdom.

ABSTRACT: To make nanomedicine potentially applicable in clinic, several methods have been developed to synthesize pure nanodrugs (PNDs) without using any additional inert carriers. In this work, we report a novel green, low-cost and scalable ice-template-assisted approach which shows several unique characteristics. Firstly, the whole process only requires adding drug solution into an ice template and subsequent melting (or freeze-drying), allowing easy industrial mass production with low capital investment. Secondly, the production yield is much higher than that of the traditional reprecipitation approach. The yield of Curcumin (Cur) PNDs is over two orders

(~ 140 times) magnitude higher than that obtained in a typical reprecipitation preparation. By adjusting simple processing parameters, PNDs with different sizes (~ 20-200 nm) can be controllably obtained. Finally, the present approach can be easily applicable for a wide range of hydrophobic therapeutic drugs without any structural modification.

KEYWORDS: mass production, pure nanodrugs, ice-template, nanomedicine

Chemotherapy plays a significant role in cancer treatment.[1-5] It can be applied before radiotherapy or surgery to shrink tumor or afterwards to destroy any remaining cancer cells. Although effective, its use is seriously hindered by many limitations such as fast renal clearance, poor bioavailability, and tremendous side effect, due to small drug molecule size,[6,7], low water solubility,[8-10] lack of tumor and cancer cell targeting, and etc.[7, 11-14] To solve these issues, in the past couple of decades, researchers have been developing approaches to package therapeutics drugs to nanomaterials. This strategy can: (1) greatly improve water dispersibility and bioavailability;[15,16] (2) dramatically enhance tumor targeting by capping nanomaterials' surface with specific ligands or by passive targeting due to the enhanced permeability and retention (EPR) effect.[17,18] The commonly employed nanomaterials include polymeric micelles,[19,20] dendrimers,[21,22] polymeric nanoparticles (NPs),[23,24] carbon based nanomaterials,[25-27] mesoporous silica NPs[28-30] and inorganic materials[31-33]. While these nanomaterials can be used as carriers to deliver anticancer therapeutics with improved efficacy, there are still issues to be addressed: (1) Despite drug-loading capacity of about 80 wt% has been achieved with some porous carriers,[34,35] drug-loading capacity in most nanocarriers is typically below 10 wt%;[36-40] (2) accumulation of large amount of excipient nanomaterials in patient's body leads to safety concerns including their metabolisms and potential long-term toxicities as well as serious inflammation.[6,10,38,41-43]

To further improve nanotechnologies to make it potentially applicable in clinic, several methods have been developed to synthesize pure nanodrugs (PNDs) without using additional inert nanomaterials.[6,10,38,40,43-56] For example, Kasai and co-workers modified the drug-solvent physical interactions by jointing two SN-38 drug molecules to form dimers and obtained PNDs upon the reprecipitation method.[44] The prepared PNDs are expected to have good stability of aqueous dispersions and improved cell penetrability over free drugs.[44] Subsequently, Yan and co-workers conjugated a hydrophobic drug and a hydrophilic drug together to form amphiphilic molecules followed by self-assembly to nanoparticles.[6] So far, the most common approach for preparing PNDs is the traditional reprecipitation (also called solvent-exchange) method,[6,43-45,47-50,54-56] in which solutions of chemotherapeutic drugs in good solvents are dropped into poor solvents and the drug molecules self-assemble into nanostructures. Apart from reprecipitation method, there are other approaches that result in drug formulations with high drug to excipient ratio, including nanocrystal technology,[57] emulsion-templated freeze drying technique[58] and surfactant-stripping.[59] Despite of the simplicity of the reprecipitation, this approach faces critical challenges including considerable batch-to-batch variations, low production rates and relatively large particle size.[47,60,61] To address these limitations, our group has developed a novel and versatile strategy for preparing PNDs via an anodized-aluminum oxide (AAO) template-assisted method.[38] This template-assisted approach produces NPs with significantly improved reproducibility and homogeneity, much higher production rate, and size tunability from 20-200 nm.[38] However, the employment of inorganic template and their removal by using acid/alkali raise concerns of undesirable contamination and damage to drugs and non-biodegradation of possible trace amount of aluminum residue. Additionally, the expensive AAO template and multiple procedures during

preparation can result in high cost in mass production. Therefore, it is essential to develop a green template for cost-effective mass production of PNDs with ultra-high purity and biocompatibility.

Herein, we report a novel ice-template-assisted approach to address the above issues. Using ice as a template has several unique merits. Firstly, PNDs can be controllably formed by dropping a drug solution into an ice template. Aqueous dispersions or solid powder of the PNDs can then be obtained by respectively melting or freeze-drying the PND-loaded ice template. Comparing to the reported AAO-template approach, the ice-template approach completely eliminates the need of employing acid or base for removal of the AAO template, which might damage the drug molecules, and cause contamination by residual aluminum. Furthermore, the production yield is much higher than that of the traditional reprecipitation approach. As a test case, Curcumin (Cur), was applied as a model hydrophobic chemotherapeutic drug in this work. Approximately 42 mg of Cur PND can be obtained, using a 10-cm diameter glass container. This yield is over two orders of magnitude (~ 140 times) higher than that obtained in a typical reprecipitation preparation (~ 0.28 mg).[38] This simple, low-capital-cost and high-yield approach enables easy industrial mass production, which is one major requirement for clinical translation of nanomedicine.

A schematic illustration of the mechanism of using ice template to prepare PNDs is presented in **Scheme 1**. A unique property of ice is that its grain boundaries contain relatively mobile water molecules, behaving like liquid,[62,63] so we exploit this characteristic to use the grain boundaries of ice for PNDs formation. Ice templates were obtained by freezing deionized water at -20 °C in a freezer or with the aid of a liquid nitrogen bath. To make PNDs, drug molecules were dissolved in an organic solvent with low boiling point, followed by dropping onto the surface of the ice template using a pipette. Upon evaporation of the organic solvent, the drug-loaded ice template was aged

for 24 hours at -20 °C to allow self-assembling of drug molecules and correspondingly formation of PNDs. Finally, simply melting or freeze-drying of the drug-loaded ice template will respectively yield a water dispersion or dry powder of PNDs (**Scheme 1**).

Scheme 1. Schematic illustration of the PNDs formation process via the ice-template-assisted strategy.

With the proposed approach, we firstly tested preparation of Cur nanodrugs. Cur is a polyphenol derived from the rhizome of *Curcuma longa* herb. It has extremely low water solubility and exhibits a wide range of pharmacological effects to many tumor cell lines.[49] In the experiment, we used a small glass container with diameter of 2.5 cm to make ice for preparation of Cur PNDs, shown in **Figure S1. Figures 1a and 1b** show respectively the SEM and TEM images of Cur PNDs with uniform spherical shape and an average diameter of ~50 nm. Dynamic light scattering measurement (DLS, **Figure 1c**) presents a hydrodynamic diameter of 55.7 nm. **Figure 1d** shows photographs of Cur in deionized water at a concentration of 40 μM (d1: pristine Cur powder; d2:

Cur PND prepared via ice template method; d3: Cur PND prepared via reprecipitation method). It can be seen that the Cur PNDs (d2 and d3) are well dispersed, while free Cur molecules cannot dissolve in water (d1).

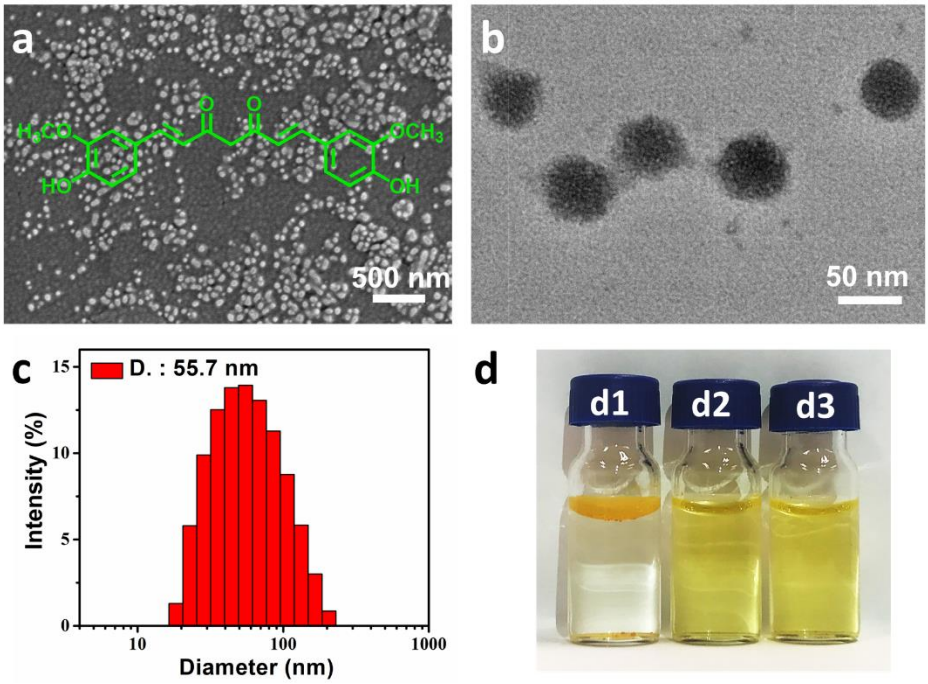

Figure 1. Characterization of Cur PNDs prepared via the ice-template-assisted strategy. a) SEM (inset: chemical structure of Cur) and b) TEM images of Cur NPs show uniform spherical particles. c) Dynamic light scattering (DLS) measurement of Cur NPs in deionized water with a diameter of 55.7 nm. d) Photographs of aqueous mixture/dispersions (40 μM) of free Cur powder (d1), Cur NPs prepared by ice-template-assisted strategy (d2) or the reprecipitation method (d3) respectively, showing much better dispersibility of NP than that of free drug molecule in water.

To further understand the PND formation mechanism and explore this method for controlling particle size, PNDs were prepared with different processing parameters (e.g. condition of ice formation, application method, temperature, concentration of drug solution). With these changing parameters, Cur PNDs of sizes from ~20 to ~200 nm can be controllably synthesized (**Figures 2 and 3**). It can be seen from **Figure 2a-d** that the size of PNDs decreases as the concentration of

the drug solution decreases. It is speculated that a higher drug concentration solution would lead to a higher local concentration within the ice grain boundary and result in larger particle sizes. When the concentration increases to be 6 mM or higher, the size of PNDs may be limited by the width of the ice grain boundary and thus the further increase of drug concentration (*e.g.* 12 mM) does not induce continual growth of particle size. Except reducing drug concentration, decreasing temperature of drug solution from 25 (**Figure 2d**) to 4 ^{o}C (**Figure 2e**) can substantially reduce the average particle size from 56 nm to 33 nm. It is proposed that when high temperature drug solution is loaded onto an ice sheet, the solution may melt the surface of its contacted ice grains and widen the grain boundary channel, leading to large PNDs (**Figure S2**). Since the grain boundary determines the size of PNDs, it is natural that the formation process of ice templates will affect particle size. Comparing to the ice formed in a common freezer at -20 ^{o}C, the ice template formed by immersion water container in a liquid nitrogen bath produces PNDs of smaller sizes (**Figure 2b** Vs **2f**). One possible explanation is that the ice formed at liquid nitrogen temperature has narrower grain boundary channels. In addition to parameter change of drug concentration, drug solution temperature, and ice formation, we found that injecting drug solution into an ice template instead of dropping (**Figure 2c** Vs **2g**) results in a smaller average diameter but a wider sizer distribution. The reason is possibly that injection will force drug solution to penetrate into a greater depth and therefore the same amount of drug molecules are more widely distributed, leading to a decreased local drug concentration and correspondingly smaller average particle size (**Figure S3**). Moreover, we investigated the morphology and size of the Cur PNDs by dropping Cur solution (1mM) into water and performing the same procedures with those for the sample in **Figure 2d** for natural evaporation of the organic solvent without ultrasound and magneton stirring. As presented in **Figure S4**, most of the resulting Cur structures display sheet structure while a small fraction of

them show nanosphere structure with size larger than 200 nm, which is quite different from that of the Cur PNDs prepared by the ice template-assisted approach (**Figure 2d**), further suggesting the confinement of the drug nanoparticle self-assembly in the grain boundaries.

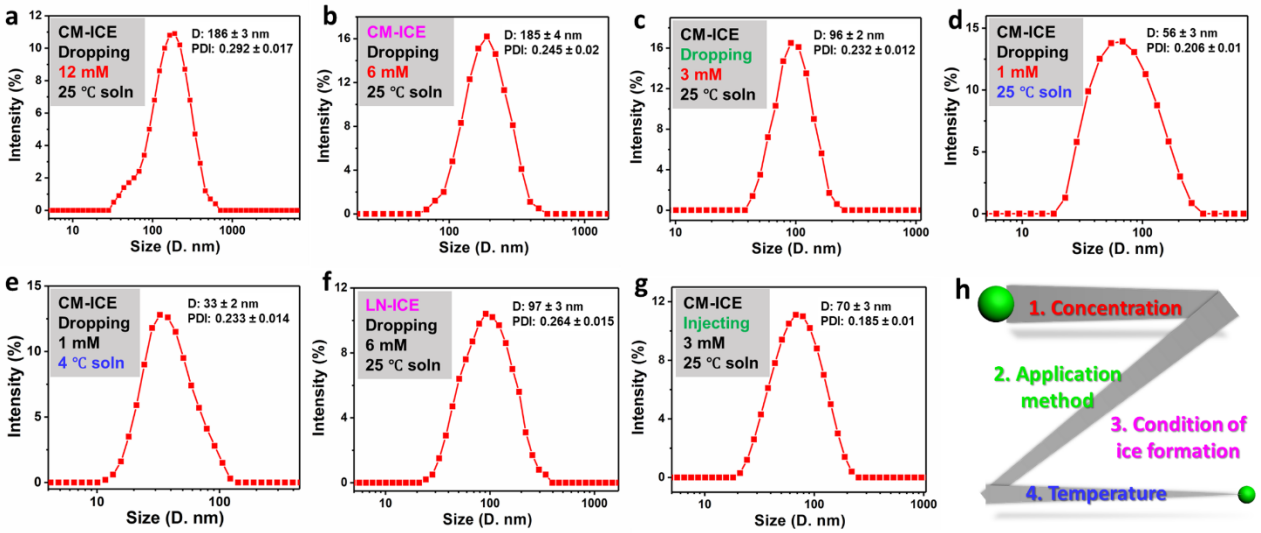

Figure 2. DLS measurements (data on right hand side, size distribution and polydispersity index (PDI) data) of Cur NPs in deionized water prepared under different conditions. CM-ICE and LN-ICE referred respectively to ice prepared with a common refrigerator at -20 ^{o}C and ice prepared by immersion in a liquid nitrogen bath. All results are expressed as mean ± standard deviation (n = 3).

As each parameter of low drug concentration, low drug solution temperature, low ice formation temperature, and great penetration depth of drug molecules generates small PNDs, it is possible to synthesize ultra-small PNDs by combining all of the 4 factors together. Therefore, we fabricated another batch of Cur PNDs by injecting a cooled (4 ^{o}C) low concentration (1 mM) of Cur drug solution into an ice template formed at liquid nitrogen temperature. Expectedly, this method generates Cur PNDs with an average size of below 20 nm, as shown in the SEM and TEM images in **Figure 3**.

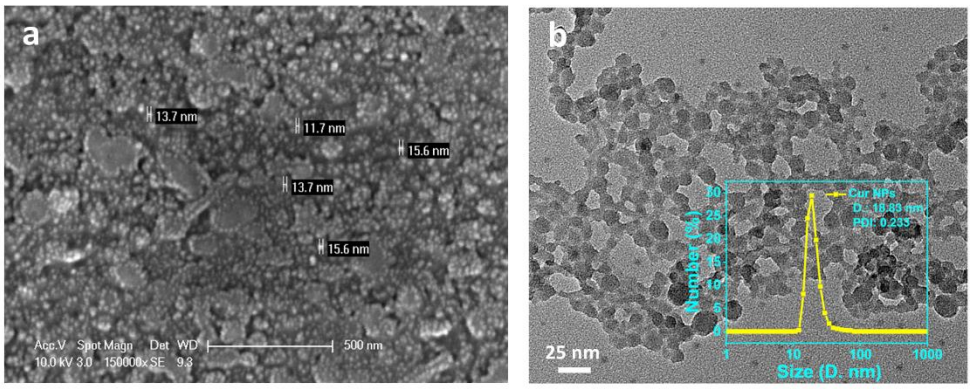

Figure 3. (a) SEM and (b) TEM images (Inset is the DLS result) of Cur PNDs with an average size of below 20 nm by injecting Cur drug solution (1 mM, 4 °C) into the ice formed in a liquid-nitrogen bath.

To explore the feasibility of the present technology for practical applications, particularly in mass production, we used a much larger ice template of 10 cm diameter. To cover the entire surface area, we injected 0.2 mL (12 mg/mL) drug solution into the ice template for 20 times (the theoretical yield is 48 mg). **Figure 4** shows different views of an ice sheet injected with Cur solution and a photograph of the produced Cur PNDs solid powder obtained by freeze drying from PND dispersions prepared from a typical run using the ice-template-assisted approach. These photographs indicate that drug solution can distribute throughout the whole surface of the ice template and has a penetration depth of about 0.5-0.7 cm. The SEM image shows that size distribution of the nanoparticles is larger (from ~30 nm to ~800 nm, average size: ~260 nm) and this is attributed to overlapping of diffusion zones of the multiple injection spots. Notably, the production yield of PND obtained via a typical run of ice-template-assisted approach is ~ 42 mg, which is over two orders (~ 140 times) higher than that obtained in a typical reprecipitation experiment (~ 0.28 mg)[38]. It should be pointed out that the actual yield (~ 42 mg) is less than the

theoretical yield (48 mg) because there are a small fraction of the drug molecules attaching to the surface of the container, thus production rate is about 87.5%. On the other hand, we also used a number of 2.5 cm glass containers to prepare the Cur PNDs in the scaled-up experiment to avoid the overlapping diffusion. To acquire the similar amount of PNDs in the above 10 cm glass container (~ 42 mg), 0.2 mL (12 mg/mL) drug solution was respectively injected into 24 glass containers with diameter of 2.5 cm for preparation of ~ 43 mg Cur PNDs (the theoretical yield is 57.6 mg, the production rate is about 74.7 %) (**Figure S5 a**). As shown in **Figure S5 b**, PNDs with smaller size and narrower distribution were obtained by using a large number of containers each received a single injection. Furthermore, using multiple injection into one single container also lead to a slightly decreased production rate. Therefore, there is a plenty of room and possibilities to improve the fabrication conditions in future industrial production.

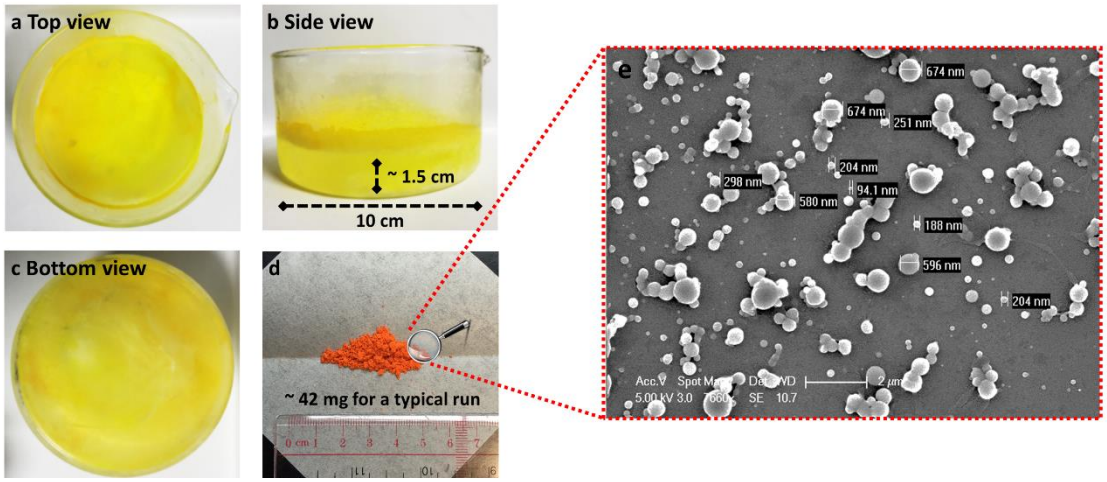

Figure 4. Top view a), side view b) and bottom view c) of an ice sheet injected with Cur solution; d) Cur PNDs powder obtained from a typical run using the ice template-assisted approach; e) SEM image of the as-fabricated Cur PND.

Besides the good potential of mass production, the proposed strategy is also applicable for a wide range of hydrophobic drug molecules. As shown in **Figures 5 a-g**, we have applied this same approach to seven other types of hydrophobic anticancer drugs including camptothecin (CPT), paclitaxel (PTX), 6-mercaptopurine (6-MP), squaraine (SQ), 5, 10, 15, 20-tetro (4-pyridyl) porphyrin (H_2TPyP), methotrexate (MTX), teniposide (VM-26). **Figure S6** displays the chemical structures of different drugs. In addition, PNDs containing synergistic drugs can also be prepared (**Figure 5 h and i**), showing that this strategy is convenient to integrate multiple drugs for performing combination therapy. We also respectively quantified the amount of drug in the supernatant and in the pellet which was obtained by low-speed centrifugation (900 rpm) for 5 min. The mass fraction of solubilized drug were determined from the mass ratio of drug in the supernatant and the pellet. All the DLS results and fraction of solubilized drug results of the as-prepared PNDs shown in **Figure 5** are summarized in **Table S1**, demonstrating good mono-dispersibility and water-dispersibility of the as-prepared nanodrugs. Furthermore, the fraction of solubilized drug of Cur PNDs suspension shown in **Figure 1** was determined to be 0.96 ± 0.03 and these values of the drugs shown in **Figure 5** are from 0.88 to 0.97 (**Table S1**), suggesting negligible large aggregates formed and good stability of the nanodrugs in the aqueous solution. The difference of these fractions may be due to the different particle size/distribution or intrinsic molecular hydrophobicity. Since removal of template with base or acid in AAO template-assisted method is not required in the ice-template-assisted strategy, there is no undesirable contamination to native drug molecules. These results suggest that the present approach is versatile and can be easily applied for preparing PNDs of single or multiple drugs in a much milder green conditions.

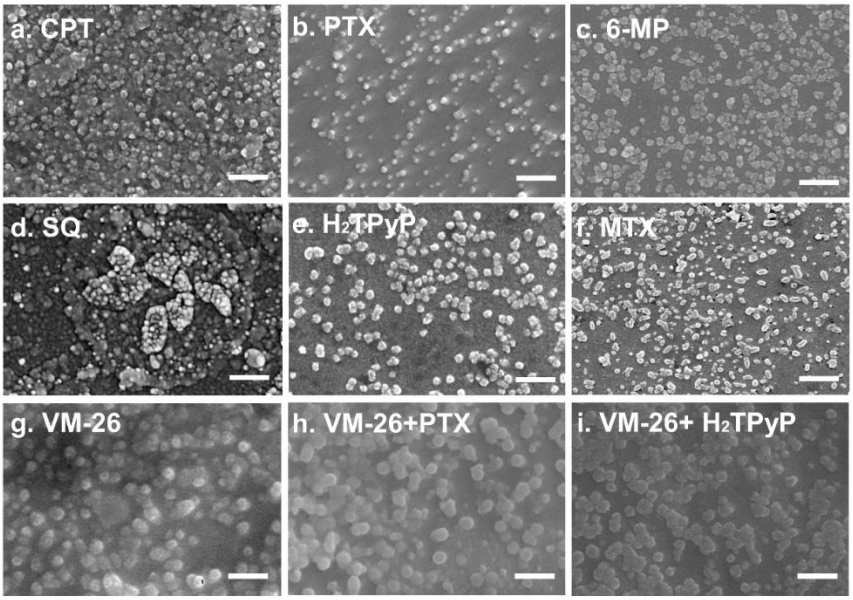

Figure 5. SEM images of a range of PNDs, indicating the universal application of ice-template-assisted strategy. a) camptothecin (CPT) b) paclitaxel (PTX), c) 6-mercaptopurine (6-MP), d), squaraine (SQ) e) 5, 10, 15, 20-tetro (4-pyridyl) porphyrin (H_2TPyP), f) methotrexate (MTX), g) teniposide (VM-26), h) VM-26 PTX PNDs, i) VM-26 H_2TPyP PNDs. Scale bar is 200 nm.

Next, to investigate biomedical profiles of the as-prepared Cur PNDs, both cellular uptake observed by confocal microscopy and *in vitro* cytotoxicity profile measured by MTT assay were carried out. As depicted in **Figure 6**, a strong cytoplasmic green fluorescence surrounding nuclei within the A549 cells is clearly observed, indicating accumulation of Cur PNDs and subsequently release of Cur molecules in cells. We next studied cytotoxicity profiles of the Cur NPs to the A549 cells compared with free Cur, the results are shown in **Figure 6**. The as-prepared Cur NPs are found to be more effective in inhibiting proliferation of the cancer cells than free Cur in all doses, which suggest that the PND formation would be more efficient for delivering anticancer drug Cur molecules inside cells compared with that of free molecule formation. These results demonstrates that the PNDs possess an apparently higher cytotoxicity than the free molecules due to more efficient internalization into cells and more released drug molecules from PNDs over the same

time. We also measured the serum stability of the as-prepared Cur PNDs in 50% fetal bovine serum (FBS) over 0, 2, 4, 6, 8, 10, 12, 24, 36, 48 h of incubation at 37°C which suggested a good stability of the as-prepared PNDs in serum (**Figure S7**), thus would be beneficial for its sustained release in blood circulation.

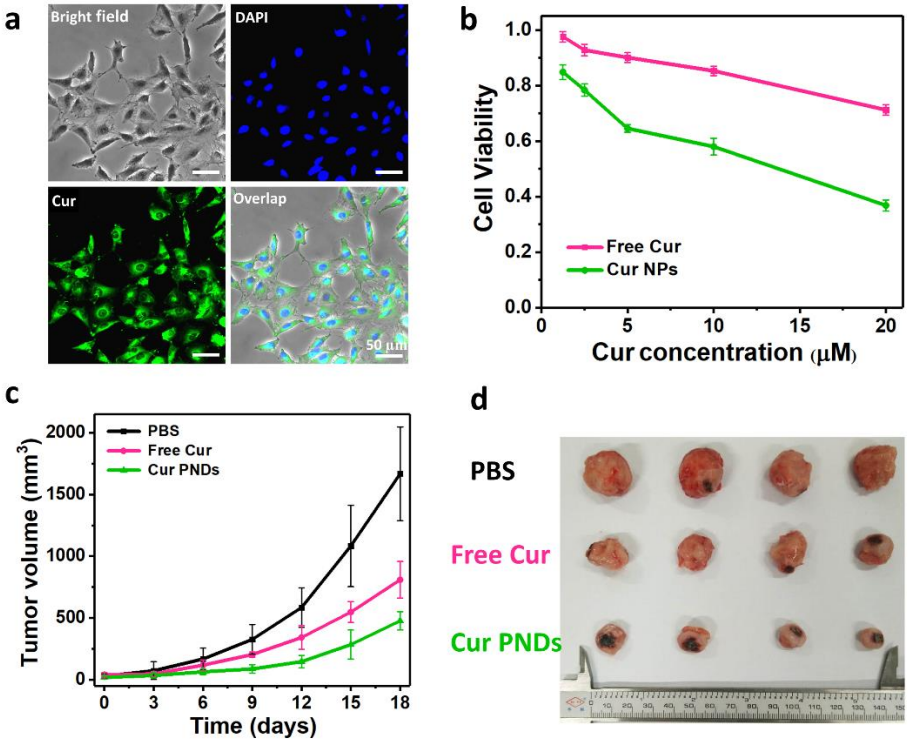

Figure 6. a). *In vitro* cell imaging and subcellular localization of the Cur NPs, monitored by fluorescence imaging in A549 cell. (Upper left) Bright filed channel; (Upper right) DAPI channel; (Lower left) Cur channel; (Lower right) Overlap of the above images. b) Cell viability of free Cur and Cur NPs in A549 cell line after 48 hours of incubation. c) *In vivo* anticancer activities of free Cur and Cur PNDs (Day 0-18). d) Representative photograph of excised tumors at the time of sacrifice from the subcutaneous tumor bearing mice after 18 days of treatments.

To further evaluate the anticancer therapeutic activities of Cur PNDs *in vivo*, the 4T1 mouse mammary tumor-bearing mice were intravenously injected with free Cur and the Cur PNDs at a Cur dose of 20 mg/kg every three days respectively when the tumors exhibited a volume of 50

mm^3. For comparison, PBS was used as a control for the intravenous injection. Tumor volumes of the tumor-bearing mice were monitored for 18 days (**Figure 6c**). **Figure 6d** shows representative photograph of excised tumors at the time of sacrifice from the subcutaneous tumor bearing mice at the end of these experiments. It can be obviously seen that mice treatment with the Cur PNDs formulation shows the best effect on suppression the tumor growth comparing with the PBS and free Cur groups. These observations are in accordance with the results of *in vitro* evaluations. All these results confirm that good anticancer therapeutic efficacy of the Cur PNDs both *in vitro* and *in vivo*.

To conclude, for the first time, we successfully developed a green, low-cost, scalable and versatile strategy for preparing PNDs via an ice-template-assisted method. We supposed the PNDs formation mechanism which is using the grain boundaries within ice matrixes as the channel for PNDs formation. By adjusting various parameters including concentration, temperature and addition way of the drug solutions as well as ice formation approach, PNDs with different sizes can be controllably obtained. This novel approach 1) has major advantages over our previously proposed AAO template in both production rate and elimination of possible metal contaminations from the template; 2) achieves mass production (~ 40 mg *vs* ~ 0.28 mg by reprecipitation, about 140 times higher than that obtained in a typical reprecipitation experiment) and size tunability (~ 20-200 nm) for Cur PNDs, which plays a crucial role in future clinical translations; 3) only requires adding of drug solution into an ice template and subsequent melting (or freeze-drying), allowing easy industrial mass production with low capital investment; and 4) can be readily extended to a wide range of hydrophobic therapeutic drugs or imaging agents without any structural modification. This work opens a new avenue for fabricating PNDs and reflects a significant advancement in developing pure nanomedicine for future clinical translations.

ASSOCIATED CONTENT

Supporting Information.

The following files are available free of charge.

Materials, experimental details, digital photographs, serum stability, schematic illustration of the PNDs formation mechanism, chemical structures of different drugs (PDF)

AUTHOR INFORMATION

Corresponding Author

E-mail: apcslee@cityu.edu.hk. (C.S.L)

E-mail: xiaohong_zhang@suda.edu.cn (X.H.Z)

Notes

The authors declare no competing financial interest.

ACKNOWLEDGMENT

C.S.L. would like to acknowledge financial support by Hong Kong Innovation and Technology Commission (Project No. ITS/372/17).

REFERENCES

1. Irvine, D. J. *Nat. Mater.* **2011**, *10*, 342−343.
2. Hubbell, J. A.; Langer, R. *Nat. Mater.* **2013**, *12*, 963−966.
3. Mura, S.; Nicolas, J.; Couvreur, P. *Nat. Mater.* **2013**, *12*, 991−1003.
4. Li, X.; Wang, X.; Zhang, J.; Hanagata, N.; Wang, X.; Weng, Q.; Ito, A.; Bando, Y.; Golberg,

D. *Nat. Commun.* **2017**, *8*, 13936−13947.

5. Ebeid, K.; Meng, X.; Thiel, K. W.; Do, A. V.; Geary, S. M.; Morris, A. S.; Pham, E. L.; Wongrakpanich, A.; Chhonker, Y. S.; Murry, D. J.; Leslie, K. K.; Salem, A. K. *Nat. Nanotechnol.* **2018**, *13*, 72−81.
6. Huang, P.; Wang, D.; Su, Y.; Huang, W.; Zhou, Y.; Cui, D.; Zhu, X.; Yan, D. *J. Am. Chem. Soc.* **2014**, *136*, 11748−11756.
7. Bhattacharyya, J.; Bellucci, J. J.; Weitzhandler, I.; McDaniel, J. R.; Spasojevic, I.; Li, X.; Lin, C. C.; Chi, J. A.; Chilkoti, A. *Nat. Commun.* **2015**, *6*, 7939−7950.
8. Allen, T. M.; Cullis, P. R. *Science* **2004**, *303*, 1818−1822.
9. Gao, L.; Liu, G.; Ma, J.; Wang, X.; Zhou, L.; Li, X. *J. Control. Release* **2012**, *160*, 418−430.
10. Shen, G.; Xing, R.; Zhang, N.; Chen, C.; Ma, G.; Yan, X. *ACS Nano* **2016**, *10*, 5720−5729
11. Chabner, B. A.; Roberts, T. G. *Nat. Rev. Cancer* **2005**, *5*, 65−72.
12. Peng, L.; Zhang, Y.; Han, L.; Zhang, C.; Wu, J.; Wang, X.; Gao, J.; Mao, Z. *ACS Appl. Mater. Interfaces* **2015**, *7*, 18628−1863.
13. Wei, W.; Zhang, X.; Chen, X.; Zhou, M.; Xu, R.; Zhang, X. *Nanoscale* **2016**, *8*, 8118−8125.
14. Zhang, F.; Zhu, G.; Jacobson, O.; Liu, Y.; Chen, K.; Yu, G.; Ni, Q.; Fan, J.; Yang, Z.; Xu, F.; Fu, X.; Wang, Z.; Ma, Y.; Niu, G.; Zhao, X.; Chen, X. *ACS Nano* **2017***, 11,* 8838−8848.
15. Rabinow, B. E. *Nat. Rev. Drug Discovery* **2004**, *3*, 785−796.
16. Salazar, J.; Ghanem, A.; Müller, R. H.; Möschwitzer, J. P. *Eur. J. Pharm. Biopharm.* **2012**, **81**, 82−90.
17. Brambilla, D.; Luciani, P.; Leroux, J. C. *J. Control. Release* **2014**, *190*, 9−14.
18. Perry, J. L.; Reuter, K. G.; Luft, J. C.; Pecot, C. V.; Zamboni, W.; DeSimone, J. M. *Nano Lett.* **2017**, *17*, 2879−2886.

19. Shi, Y.; Meel, R.; Theek, B.; Blenke, E. O.; Pieters, E.; Fens, M. H. A. M.; Ehling, J.; Schiffelers, R. M.; Storm, G.; Nostrum, C. F.; Lammers, T.; Hennink, W. E. *ACS Nano*, **2015**, *9*, 3740−3752.

20. Lang, T.; Dong, X.; Huang, Y.; Ran, W.; Yin, Q.; Zhang, P.; Zhang, Z.; Yu, H.; Li, Y. *Adv. Funct. Mater.* **2017**, *27*, 1701093−1701103.

21. Zhou, Z.; Ma, X.; Murphy, C. J.; Jin, E.; Sun, Q.; Shen, Y.; Van Kirk, E. A.; Murdoch, W. J. *Angew. Chem. Int. Ed.* **2014**, *53*, 10949−10955.

22. Wei, T.; Chen, C.; Liu, J.; Liu, C.; Posocco, P.; Liu, X.; Cheng, Q.; Huo, S.; Liang, Z.; Fermeglia, M.; Pricl, S.; Liang, X. J.; Rocchi, P.; Peng, L. *Proc. Natl. Acad. Sci. U.S.A.* **2015**, *112*, 2978−2983.

23. Zhang, J.; Yang, C.; Zhang, R.; Chen, R.; Zhang, Z.; Zhang, W.; Peng, S. H.; Chen, X.; Liu, G.; Hsu, C. S.; Lee, C. S. *Adv. Funct. Mater.* **2017**, *27*, 1605094−1605103.

24. Zhang, J.; Chen, J.; Ren, J.; Guo, W.; Li, X.; Chen, R.; Chelora, J.; Cui, X.; Wan, Y.; Liang, X. J.; Hao, Y.; Lee, C. S. *Biomaterials* **2018**, *181*, 92−102.

25. Wu, C. H.; Cao, C.; Kim, J. H.; Hsu, C. H.; Wanebo, H. J.; Bowen, W. D.; Xu, J.; Marshall, J. *Nano Lett.* **2012**, *12*, 5475−5480.

26. Chen, Y.; Xu, P.; Shu, Z.; Wu, M.; Wang, L.; Zhang, S.; Zheng, Y.; Chen, H.; Wang, J.; Li, Y.; Shi, J. *Adv. Funct. Mater.* **2014**, *24*, 4386−4396.

27. Rammohan, A.; Mishra, G.; Mahaling, B.; Tayal, L.; Mukhopadhyay, A.; Gambhir, S.; Sharma, A.; Sivakumar, S. *ACS Appl. Mater. Interfaces* **2016**, *8*, 350−362.

28. Meng, H.; Wang, M.; Liu, H.; Liu, X.; Situ, A.; Wu, B.; Ji, Z.; Chang, C. H.; Nel, A. E. *ACS Nano*, **2015**, *9*, 3540−3557.

29. Zhang, J.; Zhang, J.; Li, W.; Chen, R.; Zhang, Z.; Zhang, W.; Tang, Y.; Chen, X.; Liu, G.;

Lee, C. S. *Theranostics* **2017**, *7*, 3007−3020.

30. Wei, Q.; Chen, Y.; Ma, X.; Ji, J.; Qiao, Y.; Zhou, B.; Ma, F.; Ling, D.; Zhang, H.; Tian, M.; Tian, J.; Zhou, M. *Adv. Funct. Mater.* **2018**, *28*, 1704634−1704645.
31. Tripathy, N.; Ahmad, R.; Ko, H. A.; Khang, G.; Hahn, Y. B. *Chem. Commun.* **2015**, *51*, 2585−2588.
32. Ma, X.; Zhang, X.; Yang, L.; Wang, G.; Jiang, K.; Wu, G.; Cui, W.; Wei, Z. *Nanoscale*, **2016**, *8*, 8687−8695.
33. Chen, Y.; Song, G.; Dong, Z.; Yi, X.; Chao, Y.; Liang, C.; Yang, K.; Cheng, L.; Liu, Z. *Small* **2017**, *13*, 1602869−1602878.
34. Huxford, R. C.; deKrafft, K. E.; Boyle, W. S.; Liu, D.; Lin, W. *Chem. Sci.* **2012**, *3*, 198−204.
35. Wang, H.; Agarwal, P.; Zhao, S.; Yu, J.; Lu, X.; He, X. *Nat. Commun.* **2015**, *6*, 10081−10092.
36. Bag, P. P.; Wang, D.; Chena, Z.; Cao, R. *Chem. Commun.* **2016**, *52*, 3669−3672.
37. Wang, H.; Wang, K.; Mu, Q.; Stephen, Z. R.; Yu, Y.; Zhou, S.; Zhang, M. *Nanoscale* **2017**, *9*, 1434–1442.
38. Zhang, J.; Li, Y.; An, F. F.; Zhang, X.; Chen, X.; Lee, C. S. *Nano Lett.* **2015**, *15*, 313−318.
39. Luo, C.; Sun, J.; Liu, D.; Sun, B.; Miao, L.; Musetti, S.; Li, J.; Han, X.; Du, Y.; Li, L.; Huang, L.; He, Z. *Nano Lett.* **2016**, *16*, 5401−5408.
40. Liang, X.; Gao, C.; Cui, L.; Wang, S.; Wang, J.; Dai, Z. *Adv. Mater.* **2017**, *29*, 1703135-1703143.
41. Chung, J. E.; Tan, S.; Gao, S. J.; Yongvongsoontorn, N.; Kim, S. H.; Lee, J. H.; Choi, H. S.; Yano, H.; Zhuo, L.; Kurisawa, M.; Ying, J. Y. *Nat. Nanotechnol.* **2014**, *9*, 907−912.
42. Zhao, H.; Feng, H.; Liu, D.; Liu, J.; Ji, N.; Chen, F.; Luo, X.; Zhou, Y.; Dan, H.; Zeng, X.; Li, J.; Sun, C.; Meng, J.; Ju, X.; Zhou, M.; Yang, H.; Li, L.; Liang, X.; Chu, L.; Jiang, L.; He, Y.;

Chen, Q. *ACS Nano* **2015**, *10*, 9638−9651.

43. Zhang, R.; Xing, R.; Jiao, T.; Ma, K.; Chen, C.; Ma, G.; Yan, X. *ACS Appl. Mater. Interfaces* **2016**, *8*, 13262−13269.
44. Kasai, H.; Murakami, T.; Ikuta, Y.; Koseki, Y.; Baba, K.; Oikawa, H.; Nakanishi, H.; Okada, M.; Shoji, M.; Ueda, M.; Imahori, H.; Hashida, M. *Angew. Chem., Int. Ed.* **2012**, *51*, 10315−10318.
45. Li, W.; Yang, Y.; Wang, C.; Liu, Z.; Zhang, X.; An, F.; Diao, X.; Hao, X.; Zhang, X. *Chem. Commun.* **2012**, *48*, 8120−8122.
46. Cheetham, A. G.; Zhang, P.; Lin, Y.; Lock, L. L.; Cui, H. *J. Am. Chem. Soc.* **2013**, *135*, 2907−2910.
47. Wang, Y.; Liu, D.; Zheng, Q.; Zhao, Q.; Zhang, H.; Ma, Y.; Fallon, J. K.; Fu, Q.; Haynes, M. T.; Lin, G.; Zhang, R.; Wang, D.; Yang, X.; Zhao, L.; He, Z.; Liu, F. *Nano Lett.* **2014**, *14*, 5577−5583.
48. Zhang, J.; Liang, Y. C.; Lin, X.; Zhu, X.; Yan, L.; Li, S.; Yang, X.; Zhu, G.; Rogach, A. L.; Yu, P. K. N.; Shi, P.; Tu, L. C.; Chang, C. C.; Zhang, X.; Chen, X.; Zhang, W.; Lee, C. S. *ACS Nano* **2015**, *10*, 9741−9756.
49. Zhang, J.; Li, S.; An, F. F.; Liu, J.; Jin, S.; Zhang, J. C.; Wang, P. C.; Zhang, X.; Lee, C. S.; Liang, X. J. *Nanoscale* **2015**, *7*, 13503−13510.
50. Lee, Y.; Lee, S.; Lee, D. Y.; Yu, B.; Miao, W.; Jon, S. *Angew. Chem. Int. Ed.* **2016**, *55*, 10676−10680.
51. Xing, P.; Zhao, Y. *Adv. Mater.* **2016**, *28*, 7304−7339.
52. Cai, Y.; Shen, H.; Zhan, J.; Lin, M.; Dai, L.; Ren, C.; Shi, Y.; Liu, J.; Gao, J.; Yang, Z. *J. Am. Chem. Soc.* **2017**, *139*, 2876−2879.

53. Shamay, Y.; Shah, J.; Işık, M.; Mizrachi, A.; Leibold, J.; Tschaharganeh, D. F.; Roxbury, D.; Budhathoki-Uprety, J.; Nawaly, K.; Sugarman, J. L.; Baut, E.; Neiman, M. R.; Dacek, M.; Ganesh, K. S.; Johnson, D. C.; Sridharan, R.; Chu, K. L.; Rajasekhar, V. K.; Lowe, S. W.; Chodera, J. D.; Heller, D. A. *Nat. Mater.* **2018**, *17*, 361−368.

54. Yan, L.; Amirshaghaghi, A.; Huang, D.; Miller, J.; Stein, J. M.; Busch, T. M.; Cheng, Z.; Tsourkas, A. *Adv. Funct. Mater.* **2018**, *28*, 1707030−1707037.

55. Cong, Y.; Xiao, H.; Xiong, H.; Wang, Z.; Ding, J.; Li, C.; Chen, X.; Liang, X. J.; Zhou, D.; Huang, Y. *Adv. Mater.* **2018**, *30*, 1706220−1706230.

56. Pei, Q.; Hu, X.; Zheng, X.; Liu, S.; Li, Y.; Jing, X.; Xie, Z. *ACS Nano* **2018**, *12*, 1630−1641.

57. Junghanns, J. U. A. H.; Müller, R. H. *Int. J. Nanomedicine.* **2008**, *3*, 295−310.

58. Zhang, H.; Wang, D.; Butler, R.; Campbell, N. L.; Long, J.; Tan, B.; Duncalf, D. J.; Foster, A. J.; Hopkinson, A.; Taylor, D.; Angus, D.; Cooper, A. I.; Rannard, S. P. *Nat. Nanotechnol.* **2008**, *3*, 506−511.

59. Zhang, Y.; Song, W.; Geng, J.; Chitgupi, U.; Unsal, H.; Federizon, J.; Rzayev, J.; Sukumaran, D. K.; Alexandridis, P.; Lovell, J. F. *Nat. Commun.* **2016**, *7*, 11649.

60. Karnik, R.; Gu, F.; Basto, P.; Cannizzaro, C.; Dean, L.; Manu, K. W.; Langer, R.; Farokhzad, O. C. *Nano Lett.* **2008**, *8*, 2906−2912.

61. Kim, Y. T.; Chung, B. L.; Ma, M.; Mulder, W. J. M.; Fayad, Z. A.; Farokhzad, O. C.; Langer, R. *Nano Lett.* **2012**, *12*, 3587−3591.

62. Di Prinzio, C. L.; Nasello, O. B. *J. Phys. Chem. B* **1997**, *101*, 7687.

63. Schulson, E. M. *J. Mech.* **1999**, *51*, 21-27.

Supporting Information

Green Mass Production of Pure Nanodrugs via an Ice-Template-Assisted Strategy

Jinfeng Zhang[†,‡], *Weidong Nie*[†], *Rui Chen*[§], *Jipsa Chelora*[‡], *Yingpeng Wan*[‡], *Xiao Cui*[‡], *Xiaohong Zhang*[‖,*], *Wenjun Zhang*[§], *Xianfeng Chen*[⊥], *Hai-Yan Xie*[†], *and Chun-Sing Lee*[‡,*]

[†]School of Life Science, Beijing Institute of Technology, Beijing 100081, P. R. China.

[‡]Center of Super-Diamond and Advanced Films (COSDAF) & Department of Chemistry, City University of Hong Kong, 83 Tat Chee Avenue, Kowloon, Hong Kong SAR, P. R. China.

[§]Center of Super-Diamond and Advanced Films (COSDAF) & Department of Materials Science and Engineering, City University of Hong Kong, 83 Tat Chee Avenue, Kowloon, Hong Kong SAR, P. R. China.

[‖]Institute of Functional Nano & Soft Materials (FUNSOM), Jiangsu Key Laboratory for Carbon-Based Functional Materials & Devices, Soochow University, Suzhou, Jiangsu 215123, P. R. China.

[⊥]School of Engineering, Institute for Bioengineering, The University of Edinburgh, King's Buildings, Mayfield Road, Edinburgh EH9 3JL, United Kingdom.

Experimental Section

Materials and methods

Curcumin (Cur), 5, 10, 15, 20-tetro (4-pyridyl) porphyrin (H_2TPyP), tetrahydrofuran (THF), 3-(4, 5-Dimethylthiazol-2-yl)-2, 5-diphenyl tetrazolium bromide (MTT) and 4, 6-diamidino-2-phenylindole (DAPI) were purchased from Sigma-Aldrich. Camptothecin (CPT), paclitaxel (PTX), 6-mercaptopurine (6-MP), squaraine (SQ), methotrexate (MTX), teniposide (VM-26) were ordered from J&K Scientific Ltd. Dulbecco's modified Eagle's medium (DMEM, high glucose), fetal bovine serum (FBS), Dulbecco's phosphate buffered saline (PBS, 10X, pH 7.4), trypsin-EDTA (0.5% trypsin, 5.3 mM EDTA tetra-sodium, no phenol red), antibiotic agents penicillin-streptomycin were purchased from ThermoFisher Scientific. Milli-Q water with a resistivity higher than 18.4 MΩ·cm was collected from an in-line Millipore RiOs/Origin water purification system.

Preparation of PNDs *via* an ice-template-assisted strategy.

In a typical experiment, about 5 ml of DI water was put into a glass bottle of about 2 cm diameter. The ice template was prepared by either putting the glass bottle into a refrigerator at -20 °C or by immersing the bottle in a liquid nitrogen bath. Cur drug molecules were dissolved in THF with different concentrations (1 mM, 3 mM, 6 mM) at 0 or 25 °C. Then drug solutions were dropped by using a pipette onto the surface of ice template. As an alternative, the drug solution can also be injected into the ice template using a syringe. In these processes, it is important to maintain the surrounding temperature of the ice template (e.g. placing the ice template on a cooled pedestal) and that the ice surround should be blown with dry air after applying the drug solutions. Subsequently, the treated templates were stored at -20 °C for another 24 hours to allow for self-assembling of the PNDs. Finally, the resulting Cur PNDs can be extracted by simply melting or freeze-drying the ice and dispersed in deionized water via ultrasonication.

Besides Cur, PND of other therapeutics were also demonstrated by dropping CPT drug solution (2 mg/mL in ethanol), PTX drug solution (2 mg/mL in ethanol), 6-MP drug solution (2 mg/mL in methanol), SQ drug solution (0.167 mg/mL in methanol), H_2TPyP drug solution (3 mg/mL in THF), MTX drug solution (1mg/mL in THF), VM-26 drug solution (5 mg/mL in THF) (all at ~ 25 °C) onto surfaces of ice templates prepared by freezing at -20 °C in the refrigerator. Water dispersions of PNDs of these therapeutics were obtained by melting the ice template after solvent evaporation. The suspension was filtered through a 200-nm polycarbonate filter before SEM and DLS measurements.

Characterization of the as-prepared PNDs.

Sizes and morphologies of PNDs were investigated on a Philips XL-30 FEG SEM and a Philips CM200 FEG TEM. The SEM samples were prepared by dropping a dispersion of the PNDs onto a silicon substrate followed by natural drying and coating of a 2 nm layer of Au film. The TEM samples were prepared by dropping the PNDs dispersion onto a carbon film followed by natural drying. DLS and PDI measurements were carried out using a Malvern Zetasizer instrument.

***In vitro* uptake and cell imaging.**

A549 cells were cultured with DMEM (Gibco) supplemented with 10 % FBS (Gibco), and 1% penicillin-streptomycin (Gibco) in 5% CO_2 at 37 °C in a humidified incubator. The cells were trypsinized and resuspended on 60 mm culture plates, and 2 mL of the medium was combined with 1.0 mL cell suspension. The cells were then seeded on 6-well plates, which were then placed in an incubator at 37 °C overnight with 5% CO_2. Cur PNDs (final concentration in cell culture medium is 8 μM) were respectively added to each plate and carefully mixed. The treated cells were returned to the incubator (37 °C, 5% CO_2) for another 6 h. After incubation, the plates were washed thoroughly with sterile PBS and added DAPI as

a nucleus-locating dye for 5 min. Before observation, the cells were washed two times with sterile PBS and then fixed with 4% paraformaldehyde. Fluorescent images of the cells were recorded with a Nikon ECLIPSE 80i fluorescent microscope.

Cell cytotoxicity by MTT assay.

Cell cytotoxicity was determined by a standard MTT assay. The A549 cells were seeded into a 96-well cell-culture plate in DMEM (with 10% FBS, 1% penicillin/streptomycin) with 200 μL per well and then incubated for 24 h at 37˚C under 5% CO_2. After removing the original medium in each well, 200μl of DMEM containing predetermined concentrations of free Cur and Cur PNDs were respectively added to the designated wells. The final concentration of free Cur and Cur PNDs in each plate ranged from 5 to 20 μM. After 24 h incubation at 37 °C, the original medium in each well was removed. Subsequently, 180 μL of DMEM (without FBS) and 20 μL of MTT stock solution (5 mg/mL in sterile PBS) were added and incubated for 4 hours. Then the medium containing MTT was completely removed, followed by adding 200 μL of DMSO to each well. Cell viabilities were determined by reading the absorbance of the plates at 540 nm using a BioTek Powerwave XS microplate reader. The cells incubated with serum-supplemented medium represent 100% cell survival. Four replicate wells were run for each concentration.

***In vivo* antitumor activities.**

Balb/c mice were obtained from SPF (Beijing) Biotechnology Co., Ltd. and all animal experiments were performed in compliance with the guide of care and use of laboratory animals. 5×10^6 4T1 cells were subcutaneously injected about 9 days before commencing treatment. Estimated tumor volume was calculated using the formula: volume (mm^3) = length × $width^2/2$. When the tumors exhibited a volume of about 50 mm^3, these mice were randomly divided into three groups with five mice in each cohort. Animals

were administered with (i) PBS, (ii) free Cur, and (iii) Cur PNDs respectively via tail vein injection at a Cur dose of 20 mg/kg every three days. The tumor volume of each mouse were measured every three days during the whole period of treatment. Statistical evaluations of data were performed using the Student's t-test.

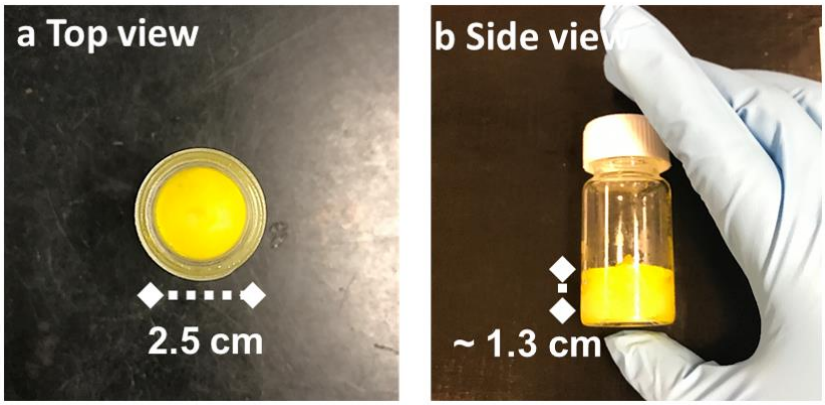

Figure S1. Top view a) and b) side view of an ice sheet dropped with a 1mM Cur solution at 25 °C.

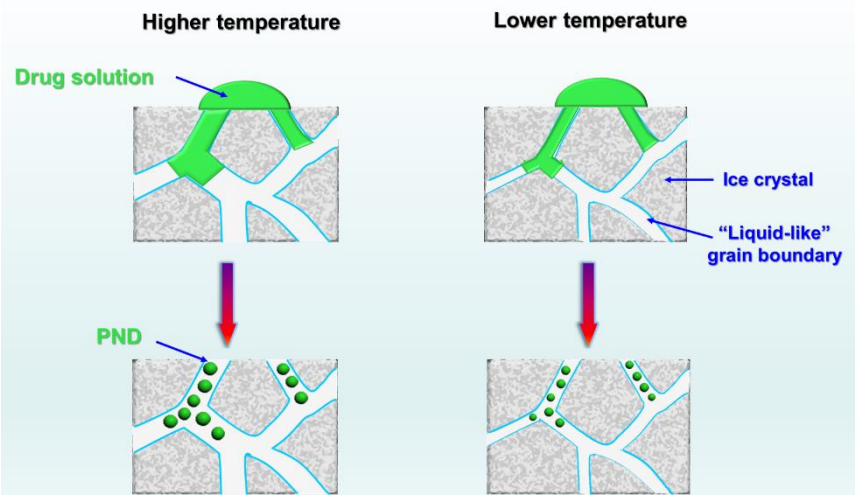

Figure S2. Schematic illustration of the PNDs formation mechanism at different temperatures via the ice-template-assisted strategy.

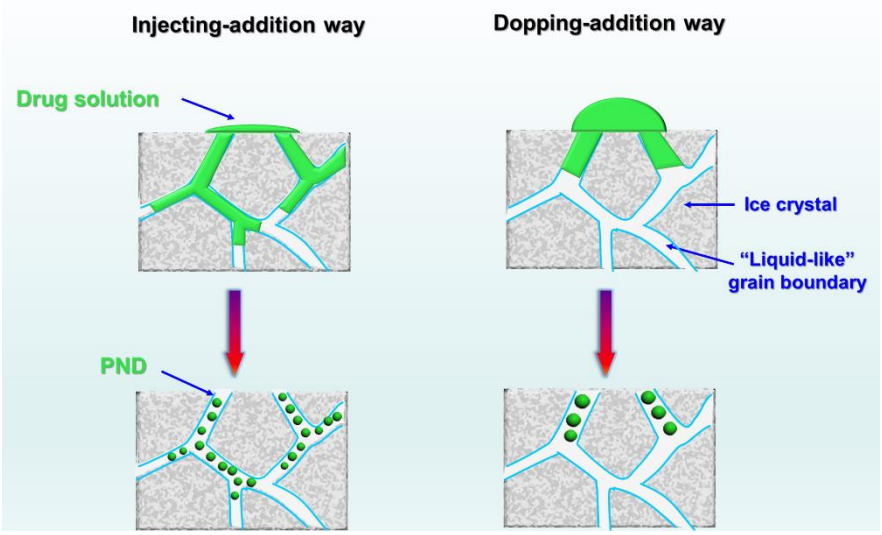

Figure S3. Schematic illustration of the PNDs formation by injection vas dropping of drug solution.

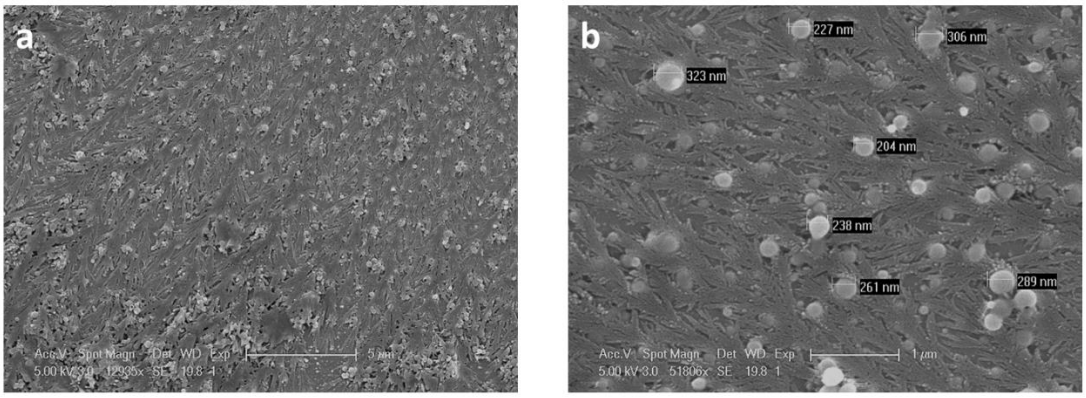

Figure S4. SEM images of Cur PNDs by dropping Cur solution (1mM) into water and removing the organic solvent via natural evaporation without ultrasound and magneton stirring.

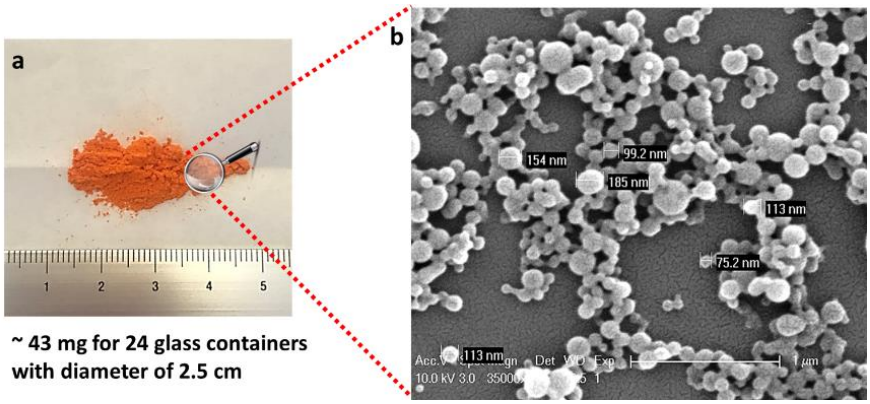

Figure S5. a) Cur PNDs powder obtained from single injection to 24 glass containers with diameter of 2.5 cm using the ice template-assisted approach; b) SEM image of the as-fabricated Cur PND.

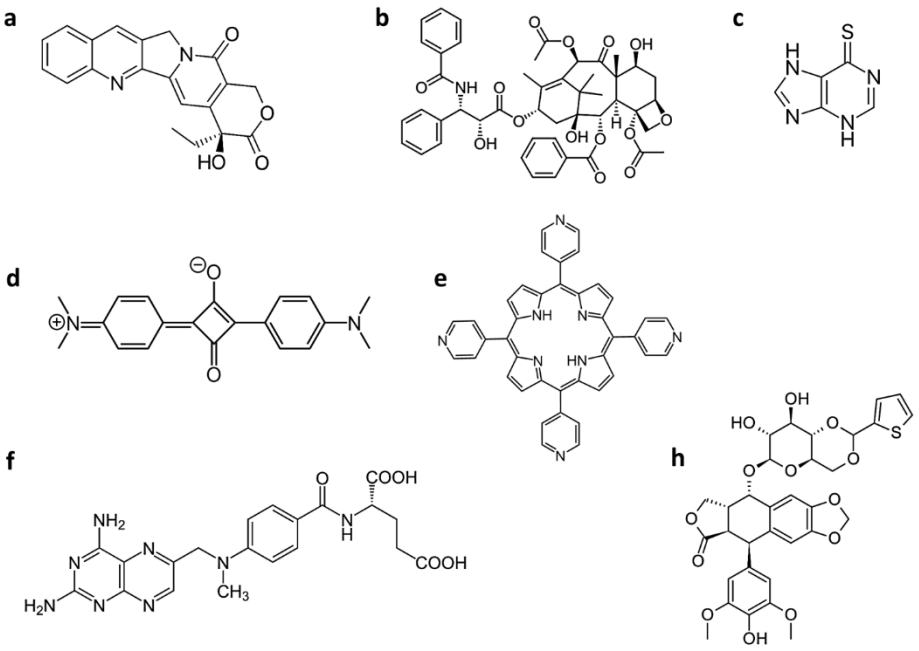

Figure S6. The chemical structures of different drugs, a) camptothecin (CPT) b) paclitaxel (PTX), c) 6-mercaptopurine (6-MP), d), squaraine (SQ) e) 5, 10, 15, 20-tetro (4-pyridyl) porphyrin (H_2TPyP), f) methotrexate (MTX), g) teniposide (VM-26).

PND	Size (Diameter)	Polydispersity index (PDI)	Mass fraction of solubilized drug
CPT	58.7 ± 3 nm	0.247 ± 0.04	0.97 ± 0.02
PTX	52.5 ± 2 nm	0.164 ± 0.02	0.94 ± 0.03
6-MP	57.3 ± 3 nm	0.209 ± 0.03	0.93 ± 0.04
SQ	34.6 ± 3 nm	0.261 ± 0.03	0.92 ± 0.03
H_2TPyP	65.4 ± 2 nm	0.183 ± 0.03	0.88 ± 0.03
MTX	55.1 ± 4 nm	0.285 ± 0.04	0.90 ± 0.05
VM-26	94.8 ± 3 nm	0.244 ± 0.02	0.95 ± 0.03
VM-26+PTX	83.9 ± 2 nm	0.211 ± 0.02	0.94 ± 0.03
VM-26+H_2TPyP	81.3 ± 3 nm	0.23 ± 0.03	0.89 ± 0.04

Table S1. DLS results and fractions of solubilized drug of the different PNDs prepared by using the ice template-assisted approach shown in **Figure 5**.

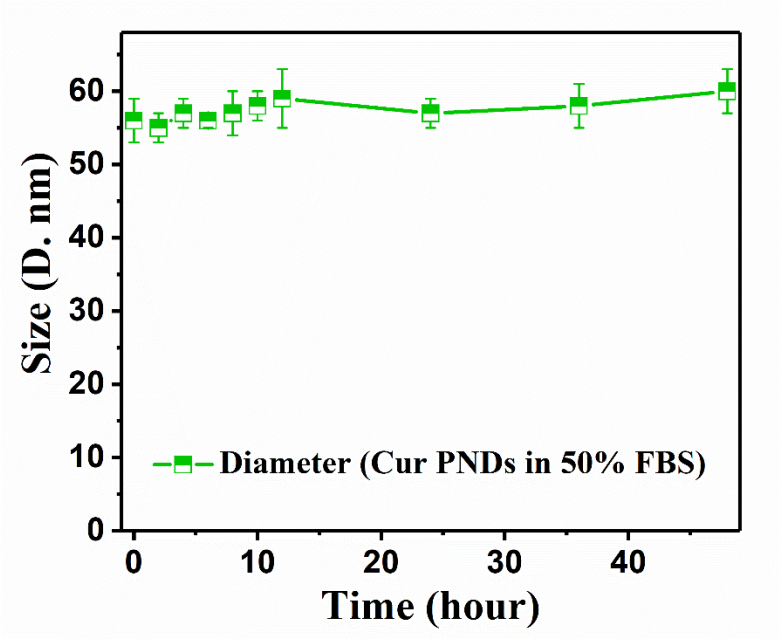

Figure S7. Serum stability of the Cur PNDs in 50% fetal bovine serum (FBS) over 0, 2, 4, 6, 8, 10, 12, 24, 36, 48 h of incubation at 37°C.